International Journal of Solids and Structures 222–223 (2021) 111036

Contents lists available at ScienceDirect

International Journal of Solids and Structures

journal homepage: www.elsevier.com/locate/ijsolstr

Effect of plasticity on the coefficient of restitution of an elastoplastic sphere impacting an elastic plate

Q. Peng [a,b], Y. Jin [a,b], X. Liu [a,b,*], Y.G. Wei [c]

[a] LNM, Institute of Mechanics, Chinese Academy of Sciences, Beijing 100190, China
[b] School of Engineering Science, UCAS, Beijing 100049, China
[c] College of Engineering, Peking University, Beijing 100871, China

ARTICLE INFO

Article history:
Received 7 January 2021
Received in revised form 13 March 2021
Accepted 19 March 2021
Available online 26 March 2021

Keywords:
Sphere-plate impact
Contact plasticity
Modified Zener model
Coefficient of restitution
Thickness dependent COR

ABSTRACT

A sphere impacting a plate is different from impacting a half-space bulk, because energy in the former case can be dissipated in a form of flexural wave propagating on the plate. Such energy loss by the elastic wave can be explained by the Zener model; however, this model is only valid for low-velocity impact with elastic Hertzian contact law. For high-velocity impact with contact plasticity, the Zener model is not valid any ore because energy dissipation by plasticity may take a large fraction, so that the Zener model, which ignores plasticity, will overestimate the coefficient of restitution (COR). In order to study how much the plasticity affects the sphere impacting the plate, we developed a modified Zener model by employing the contact plasticity into the controlling equation. Using the developed model, we firstly presented a thickness-dependent yielding velocity (yielding impact velocity depends on the thickness of the plate), above which the contact plasticity should be taken into account. What is more, we presented a semi-analytical solution to predict the COR over a large range of plate thickness. Meanwhile, finite element simulations were carried out to prove that the present model can give enough accuracy for the high velocity impact.

1. Introduction

During the impact of a spherical object on a massive object, it is interesting to see how the initial kinetic energy is partitioned during and after the impact. There will be three parts for the partition: the kinetic energy restored after rebounding, the energy by the elastic wave propagating on the plate, and the plastic energy dissipation during the impact. The first term, rebounding energy, can be used to determine the coefficient of restitution (COR). The second term, energy dissipated by elastic wave, has been studied by Hunter (Hunter, 1957) and Reed (Reed, 1985). Their results indicate that only a small fraction of energy will be converted into the elastic wave, less than 5 percent. The third term, plastic dissipation, has been noticed by Hutchings (Hutchings, 1979), and extensively studied by Thornton's group (Hutchings, 1979; Wu et al., 2003, 2005), whose study for the plastic impact showed that the energy loss due to stress wave propagation was negligible compared with the energy dissipation by plastic deformation. In all these studies, they used a half space to represent the impacted object, so that these models cannot be used for a thin plate on which the flexural wave effect can be enormous.

When the plate is thin, the half-space assumption is no longer correct. Considering the flexural wave on the plates, Zener derived the governing equation of the relative displacement for the elastic contact between the sphere and the plate (Zener, 1941). Because the Hertzian contact is used (the force is proportional to the displacement to the power of 1.5), the governing equation of Zener model cannot be analytically solved. As a result, numerical integration method was used to solve Zener model (Mueller et al., 2015; Muller et al., 2016; Zener, 1941). Results showed that the Zener model provided enough accuracy for an elastic contact under the condition that the spherical object had to be detached from the plate before the arrival of the first reflected wave from the boundary. One step further, by simplifying the force–displacement relation with a linear relationship, Mueller et al. proposed a semi-analytical solution, reaching an approximation to the Zener model for the range of COR larger than 0.2 (Mueller et al., 2015).

There are also a few studies concerning the thickness effect of the plate. For a thick plate (Mittal, 1987) or a thick beam (Sherif and Almufadi, 2018), the transverse shear deformation cannot be neglected. For instance, Mittal proposed a closed form solution to determine the deflection of the impact point (Mittal, 1987). For

* Corresponding author at: LNM, Institute of Mechanics, Chinese Academy of Sciences, Beijing 100190, China.
E-mail address: xiaomingliu@imech.ac.cn (X. Liu).

https://doi.org/10.1016/j.ijsolstr.2021.03.023
0020-7683/

Nomenclature

FEM	Finite element method
NFD	Normal-force displacement
COR	Coefficient of restitution
e	Coefficient of restitution
E_1	Young's modulus of the sphere
E_2	Young's modulus of the plate
E^*	Effective modulus
F_m	Maximum force during loading stage
$F(\delta)$	Function for the normal-force displacement relationship
$F(x_1;x_2,x_3)$	Equivalent form of $F(\delta)$ for present dynamical system
H	Thickness of the plate
m^*	Effective mass
R	Radius of the sphere
R^*	Effective radius
R_e	Residual for Taylor expansion
t	Time
V_0	Initial impact velocity of the sphere
V_W	Propagation velocity of longitudinal waves
V_r	Recovered velocity of the sphere
V_{Y0}	Yielding velocity of a sphere impacting a bulk
V_Y	Yielding velocity of a sphere impacting a plate
w	Dimensionless compressive relative displacement
w_m	Maximum dimensionless compressive relative displacement
x_1, x_2, x_3	State variables for present dynamical systemState variables for present dynamical system
δ	Compressive relative displacement
δ_m	Maximum compressive relative displacement
δ_r	Residual compressive relative displacement
δ_Y	Yielding compressive relative displacement
δ_P	Transition parameter for elastic and elastoplastic loading
ρ_1	Density of the sphere
ρ_2	Density of the plate
ν_1	Poisson's ratio of the sphere
ν_2	Poisson's ratio of the plate
λ	Zener's inelasticity parameter
η	One material-dependent parameter
σ_Y	Yielding strength of the sphere

an even thicker plate, the wave reflection from the opposite side of the plate should also be considered; the bending of the plate is achieved by at least 6–8 wave transitions (Boettcher et al., 2017; Koller and Kolsky, 1987).

In the experiment of a sphere impacting a half space, authors can record the contact force history to evaluate the surface deformation. Sherif and Almufadi used a thick block to represent an infinite half space and a linear model to consider the contact plasticity (Sherif and Almufadi, 2018). Once the force history was recorded, the displacement of the sphere can be integrated using elastic or plastic contact model. The experiment of a sphere impacting a thin plate, on the contrary, is different from a sphere impacting a half space, because the slenderness has to be considered during the contact. Muller et al. experimentally measured the history of a steel spheres impacting a sufficiently large glass plate and then compared the result with the Zener model (Muller et al., 2016). They concluded that, compared with experiment, the Zener model might underestimate the contact time for thin plates (for example, the ratio of plate thickness to sphere radius is less than 0.3). It should be noticed that they mainly focused on low-velocity impact, so that the plasticity effect on the contact had not be discussed.

The Zener model has enough accuracy as long as the impact remains elastic. For impacts with higher velocity, plastic deformation cannot be ignored, a lot of studies has proposed the plastic contact models. For example, Johnson's contact model is suitable for elastic perfect-plastic contact (Johnson, 1985). The Jackson–Green (JG) (Jackson and Green, 2005) and Kogut–Etsion (KE) (Kogut and Etsion, 2002) models are suitable for the contact between a rigid flat surface and deformable hemisphere. The Kogut–Komvopoulos (KK) (Kogut and Komvopoulos, 2004), Ye–Komvopoulos (YK) (Ye and Komvopoulos, 2003), Brake (Brake, 2012, 2015), Stronge (Stronge, 2000), Thornton (Thornton, 1997), and modified version of the JG models (Ghaednia et al., 2015) are suitable for the contact between a rigid hemisphere and a deformable half space.

Previous plasticity contact models have been used for cases such as sphere-half space impact (Thornton, 1997), rough surface contact (Majumdar and Bhushan, 1991), rod contact (Ghaednia et al., 2015; Ye et al., 2020). However, few studies have been focused on the mixed effect of the plasticity and flexural wave on the thin plate impact. Patil and Higgs has paid attention to the effect of both the plasticity and flexural vibration on the COR for sphere-plate contact (Patil and Higgs, 2017). Similar to Mueller's linearization method of the normal force–displacement (NFD) relationship, they proposed a linear normal force–displacement relationship for the plastic phase so that a semi-analytical approach was possible. The flexural wave effect has also been investigated on plastic impacts of a sphere against a slender beam (Wang et al., 2017a, 2017b). The authors used different contact models to check the vibration effect induced by impacts theoretically and experimentally. Their results suggested Hertz model matches the experiment well under the condition of low impact velocities. For higher-velocity impact, they suggested that plastic contact model shall be used, and under such condition, responses of the flexible beam become very sensitive to the selection of the contact model.

In summary, on one hand, for high velocity sphere impacting a half space, previous studies have concluded that the COR is proportional to $V_0^{-0.5}$ (V_0: initial impact velocity of the sphere) as a result of plasticity (Wu et al., 2003, 2005). On the other hand, for an elastic sphere impacting a thin plate, the COR monotonically depends on the Zener's parameter λ which is proportional to $V_0^{0.2}$ (Mueller et al., 2015; Muller et al., 2016; Zener, 1941). It is still not clear how the COR changes with V_0 for the plastic impact between a sphere and a thin plate. Aiming to discover this effect, present study deals with the impact during which both the plasticity and flexural wave effect should be considered. By using the developed model in this work, we discuss how much is the dependency of the COR on the impact velocity V_0 if both factors—the plasticity and wave effects—are considered. The paper is organized as follows. First, we built an elastoplastic contact model for the sphere-plate impact from finite element simulation. Second, we modified Zener model with the elastoplastic contact model to a 3-variable first-order dynamical system. Using the modified model, we first obtained the yield velocity, above which the plasticity should be taken into account. What is more, we obtained a semi-analytical expression for the COR depending on the impact velocity, and further validated the solution with finite element simulations. Last, we also discussed the effect of plasticity on energy dissipation and contact duration.

2. Description of problem

Fig. 1 illustrates the process of an elastoplastic sphere impacting an elastic plate. The sphere hits the plate with initial impact velocity of V_0, and then decelerates to zero by the reaction force. At this moment, the sphere arrives its maximum compressive relative displacement δ_m to the plate; the plate, on the other hand, deforms to an extent depending on its compliance. Next, during the restitution stage, the sphere bounces back, and the flexural wave continues travelling further away from the impact location. Finally, the sphere detaches from the plate with a recovered velocity V_r before the flexural wave could reflect back from boundary (the radius of the plate is sufficiently large). A permanent compressive relative displacement δ_r remains if plastic deformation takes place. Under such condition, the loss of kinetic energy will compose of two parts: the flexural wave and the plastic dissipation.

The motion of the sphere is governed by the following equation with respect to the compressive relative displacement δ (Zener, 1941).

$$\frac{\mathrm{d}^2\delta}{\mathrm{d}t^2}+\frac{1}{m^*}F(\delta)+\alpha\frac{\mathrm{d}F(\delta)}{\mathrm{d}t}=0 \tag{1}$$

where m^* is the effective mass

$$m^*=\left(\frac{1}{m_1}+\frac{1}{m_2}\right)^{-1}$$

m_1 the mass of the sphere, m_2 the mass of the plat, α a constant

$$\alpha=\frac{\sqrt{\frac{3\rho_2\left(1-\nu_2^2\right)}{E_2}}}{4\rho_2 H^2}$$

H the thickness of the plate, ρ_2 the density of the plate, ν_2 the Poisson's ratio of the plate, E_2 the Young's modulus of the plate and $F(\delta)$ the normal contact force depending on δ. Zener used the Hertzian contact model to derive a model for the COR for small λ, which is an inelasticity parameter with the form

$$\lambda=\frac{\pi^{\frac{3}{5}}}{3^{\frac{1}{2}}}\left(\frac{R}{H}\right)^2\left(\frac{V_0}{V_W}\right)^{\frac{1}{5}}\left(\frac{\rho_1}{\rho_2}\right)^{\frac{3}{5}}\left(\frac{E_1/(1-\nu_1^2)}{E_1/(1-\nu_1^2)+E_2/(1-\nu_2^2)}\right)^{\frac{2}{5}} \tag{2}$$

where $V_W=\sqrt{E_2/\rho_2(1-\nu_2^2)}$ is the propagation velocity of longitudinal waves in the thin plate (Landau et al., 1986), R the radius of the sphere, H the thickness of the plate, V_0 the impact velocity, E_1 the Young's modulus of the sphere, and ν_1 the Poisson's ratio of the sphere, and ρ_1 the density of the sphere. By using a linearization method, Mueller et al. (Mueller et al., 2015) obtained an approximate solution, in which the COR was given by

$$e=\exp\left(-\pi\frac{\lambda}{\sqrt{4-\lambda^2}}\right) \tag{3}$$

However, if the impact velocity exceeds the yielding velocity (Thornton, 1997), plastic deformation will take place such that the Hertzian NFD relationship is no longer valid. Under the assumption that the kinetic energy of the sphere is solely dissipated by plastic deformation, Thornton adopted the expression $V_{Y0}=3.194\sqrt{\sigma_Y^5R^{*3}/E^{*4}m^*}$ for this yielding velocity which was first obtained by Davies (Davies, 1949), where σ_Y is the yielding strength, R^* the effective radius, and E^* the effective modulus (Thornton, 1997). By Thornton's assumption, the yielding velocity was determined by the yielding compressive relative displacement δ_Y. However, the yielding compressive relative displacements are generally not necessarily the same for different elastoplastic contact models. For example, other than $\delta_Y=0.25\pi^2\sigma_Y^2R^*/E^{*2}$ provided by Thornton, Majeed et al. (the MYC model) suggested that $\delta_Y=0.68\pi^2\sigma_Y^2R^*/E^{*2}$ (Majeed et al., 2012). Following Thornton's assumption, we can obtain the yielding velocity according to the MYC model (Majeed et al., 2012):

$$V_{Y0}=0.552\sqrt{\frac{\pi^4\sigma_Y^5}{\rho_1E^{*4}}} \tag{4}$$

For an elastoplastic γAl_2O_3 sphere with $R=0.9$mm impacting an elastic glass bulk (Muller et al., 2016), we can calculate the yielding velocity being 2.126 m/s and 7.426 m/s using Thornton's model and Eq. (4), respectively, indicating that we have to select a suitable elastoplastic contact model first to model the dynamics.

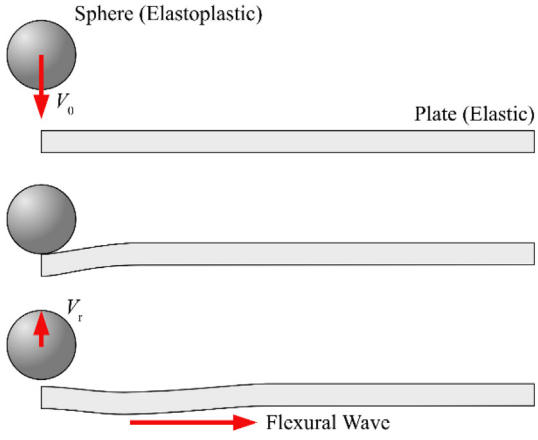

Fig. 1. Schematic diagram for an elastoplastic sphere impacting an elastic plate.

3. Modified Zener's model considering plasticity

3.1. Choice of elastoplastic NFD relationship

Different contact models generally lead to different results for either the loading stage or the unloading stage (Wang et al., 2017b), including the history of contact force, the contact duration, and as we showed in Section 2, the yielding velocity. To find a correct NFD relationship for elastoplastic contact, we built a Finite Element Method (FEM) model to inspect NFD relationships. FEM simulations were carried out using commercial software ABAQUS with a static solver (ABAQUS/Standard). Due to the symmetry, only an axisymmetric model was used, as shown in Fig. 2. The radius of the sphere R is set to 0.9 mm. The width and thickness of the bulk were set to $500R$ in order to eliminate the boundary effects. A contact pair was established between the sphere and the plate: the penalty method of constraint enforcement was applied on the normal direction for the pressure-overclosure relationship ('Hard' contact in ABAQUS), and the friction coefficient was set to 0.1 (ABAQUS, 2016).

In this study, we investigated an elastoplastic sphere in contact with an elastic target. As an example, we set the materials for the elastic-perfect plastic sphere and the elastic plate to γAl_2O_3 and glass, respectively, which were also experimentally studied by Mueller et al. (Mueller et al., 2015). Table 1 lists the details of the material parameters for the FEM model. The sphere and the bulk were meshed with linear element CAX4R with element count more than 70,000 and the finest element size at the contact region being $0.01R_1$ (Peng et al., 2020).

With this model, by simulation of both loading and unloading processes, we obtained both an elastic and an elastoplastic NFD relationships, shown in Fig. 3. Results show that the MYC model

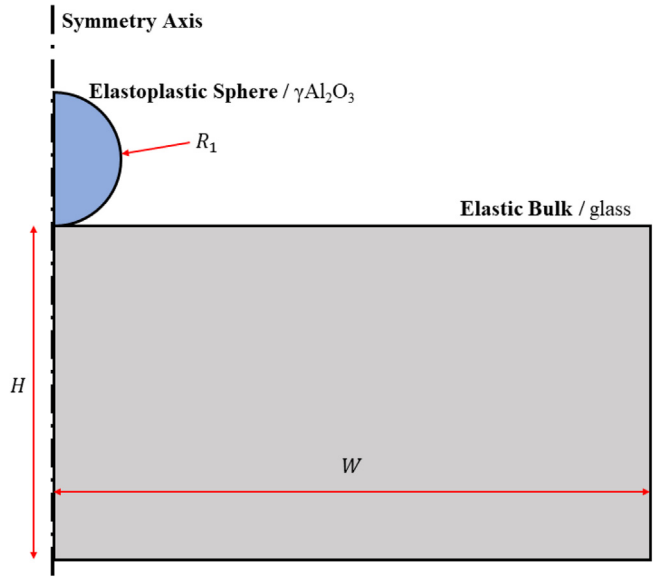

Fig. 2. Schematic diagram for validation of elastoplastic contact models.

Table 1
Material Properties for FEM model.

	Sphere	Bulk
Material	γAl_2O_3	glass
Young's Modules (GPa)	12.23	73
Poisson Ratio	0.21	0.21
Density (kg/m^3)	879	2500
Yielding Stress (MPa)	472.5	N/A

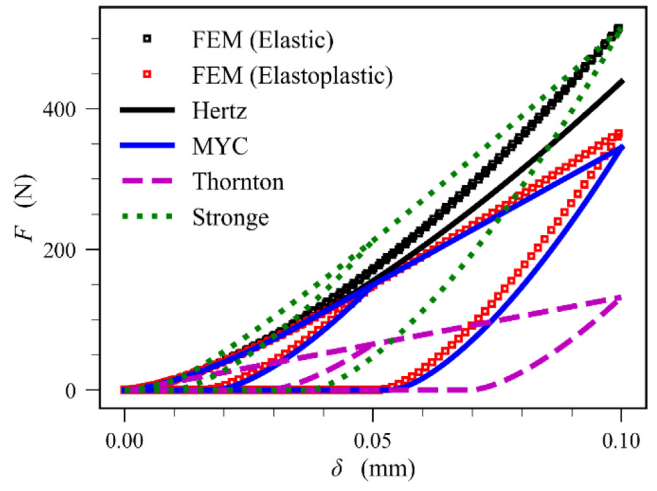

Fig. 3. Validation of various models with FEM simulation.

(Majeed et al., 2012) matches the FEM results with an error less than 6%, while the Hertzian law only works in the elastic regime with very small compressive relative displacement, the Thornton model (Thornton, 1997; Wang et al., 2017b) underestimates the contact force about 64%, and the Stronge model (Stronge, 2019; Wang et al., 2017b) overestimate the contact force about 40%. Based on such comparison, we selected the MYC model for the NFD function $F(\delta)$. It should be noted that previous study by Wang also considered the MYC model as their best choice in the study of dynamic elastoplastic contact of a sphere and a beam (Wang et al., 2017a). Similarity, Dong et al. showed that the MYC model can bring higher accuracy in the prediction of the COR under high-speed impact ($V_0 \geq 1.6$m/s in their study) (Dong et al., 2018).

With the MYC model, we used the contact force as a function of the relative distance between the sphere and the plate, so that permanent change of sphere curvature was not explicitly considered. However, the change of the sphere shape during the contact is considered in the MYC equation. As the compressive displacement reaches the different yielding stage, different level of permanent deformation occurs. As a result, the force–displacement response in the recovery stage depends on the amplitude of plastic deformation, and also should be obviously different from that in the loading stage. In this sense, we could say that the MYC model is aware of curvature change in terms of permanent deformation.

3.2. Semi-analytical model for thickness-dependent yielding velocity

As stated in Section 2, the yielding velocity V_{Y0} used by Thornton (Thornton, 1997) or by Eq. (4) is valid only when the target is infinitely thick (bulk). For a thin plate, because of its compliance, a fraction of the kinetic energy is converted into flexural wave, so the velocity required to trigger plasticity is larger than the one for the bulk: the thinner the plate is, the larger the yielding velocity is. In this section, we investigate the thickness-dependency of the yielding velocity. The idea is that we first establish a relationship between the impact velocity V_0 and the maximum compressive relative displacement δ_m, and then by setting $\delta_m = \delta_Y$, we can obtain the relationship between the yielding impact velocity and the plate thickness.

By substitution of variables, $\delta = R\left(\frac{\pi\rho_1}{E^* V_0^{0.5}}\right)^{0.4} V_0 w$ and $t = R\left(\frac{\pi\rho_1}{E^* V_0^{0.5}}\right)^{0.4}\tau$, Eq. (1) can be expressed to the following dimensionless form,

$$\frac{d^2 w}{d\tau^2} + \left(1 + \lambda\frac{d}{d\tau}\right) w^{1.5} = 0 \tag{5}$$

and with the initial conditions

$$w|_{\tau=0} = 0$$

$$\frac{dw}{d\tau}_{\tau=0} = 1$$

By solving Eq. (5) numerically with Runge-Kutta method (Dormand and Prince, 1980; Shampine, 1986), we can find a relationship between the maximum value of w, denoted with w_m, with λ, shown as blue squares in Fig. 4. Such relationship can be linearly

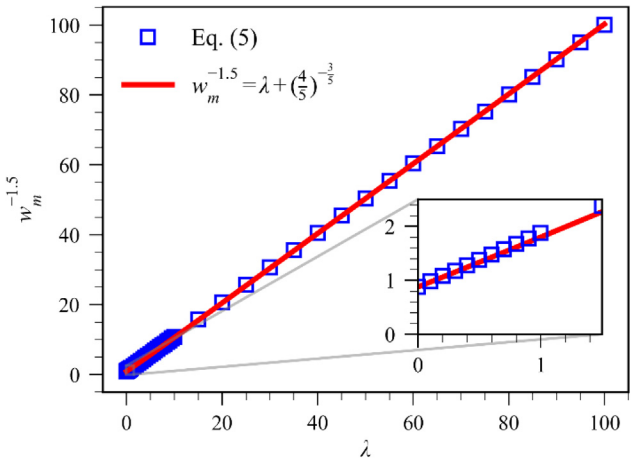

Fig. 4. $w_m^{-1.5}$ as function of λ.

approximated by $w_m^{-1.5} = c_1\lambda + c_2$, with c_2 being the value of $w_m^{-1.5}$ at $\lambda = 0$. Setting $\lambda = 0$ in Eq. (5), integration by parts reveals that $c_2 = (5/4)^{-\frac{3}{5}}$. Fitting with least squares method, we obtain $c_1 \approx 1.00$, and then the final expression for $w_m^{-1.5}$:

$$w_m^{-1.5} = \lambda + \left(\frac{5}{4}\right)^{-\frac{3}{5}} \tag{6}$$

or equivalently,

$$\delta_m = V_0 R\left(\frac{\pi\rho_1}{E^* V_0^{0.5}}\right)^{0.4}\left(\lambda + \left(\frac{5}{4}\right)^{-\frac{3}{5}}\right)^{-\frac{2}{3}} \tag{7}$$

where δ_m is the maximum compressive relative displacement.

With Eq. (7), the thickness-dependent yielding velocity V_Y can be obtained by the following equation:

$$V_Y R\left(\frac{\pi\rho_1}{E^* V_0^{0.5}}\right)^{0.4}\left(\lambda + \left(\frac{5}{4}\right)^{-\frac{3}{5}}\right)^{-\frac{2}{3}} = \delta_Y \tag{8}$$

where $\delta_Y = 0.68\pi^2\sigma_Y^2 R^*/E^{*2}$ is the yielding compressive relative displacement in the MYC model (Majeed et al., 2012). Dividing both sides of Eq. (8) by V_{Y0} gives the following equation.

$$\left(\frac{4}{5}\right)^{\frac{2}{5}}\left(\frac{V_Y}{V_{Y0}}\right)^{\frac{4}{5}}\left(\lambda + \left(\frac{5}{4}\right)^{-\frac{3}{5}}\right)^{-\frac{2}{3}} = 1 \tag{9}$$

Substituting Eq. (2) to Eq. (9) and introducing a new material-dependent coefficient,

$$\eta = \frac{\pi^{\frac{3}{5}}}{3^{\frac{1}{2}}}\left(\frac{\rho_1}{\rho_2}\right)^{\frac{3}{5}}\left(\frac{E_1/(1-\nu_1^2)}{E_1/(1-\nu_1^2) + E_2/(1-\nu_2^2)}\right)^{\frac{2}{5}}\left(\frac{V_{Y0}}{V_W}\right)^{\frac{1}{5}} \tag{10}$$

we thus obtained the relationship between V_Y/V_{Y0} and R/H as follows.

$$\left(\frac{R}{H}\right)^2 = \left(\frac{4}{5}\right)^{\frac{3}{5}}\left(\frac{V_Y}{V_{Y0}} - \left(\frac{V_Y}{V_{Y0}}\right)^{-\frac{1}{5}}\right)\frac{1}{\eta} \tag{11}$$

To estimate the yielding velocity for a given plate thickness, it is convenient to find an explicit expression for V_Y/V_{Y0} as a function of R/H and η. However, Eq. (11) cannot be solved algebraically for arbitrary η. Thus, here we propose an approximation for $V_Y/V_{Y0} \in [1, \infty)$. Eq. (11) can be rewritten as follows.

$$\begin{cases} \frac{V_Y}{V_{Y0}} - q = \left(\frac{V_Y}{V_{Y0}}\right)^{-\frac{1}{5}} \\ q = \eta\left(\frac{5}{4}\right)^{\frac{3}{5}}\left(\frac{R}{H}\right)^2 \end{cases} \tag{12}$$

If we can convert the term $(V_Y/V_{Y0})^{-\frac{1}{5}}$ to a function of R/H, then the desired explicit expression can be obtained. To do that, we expand $(V_Y/V_{Y0})^{-\frac{1}{5}}$ at a carefully selected location, $V_Y/V_{Y0} = q + 1$, as follows.

$$\left(\frac{V_Y}{V_{Y0}}\right)^{-\frac{1}{5}} = (q+1)^{-\frac{1}{5}} + \sum_{n=1}^{\infty} a_n \frac{\left(\frac{V_Y}{V_{Y0}} - q - 1\right)^n}{(q+1)^{\frac{1}{5}+n}}$$

where a_n is the coefficients of Taylor expansion and $|a_n| < 1$. Finally, we obtain the approximation for V_Y/V_{Y0}.

$$\frac{V_Y}{V_{Y0}} = \eta\left(\frac{5}{4}\right)^{\frac{3}{5}}\left(\frac{R}{H}\right)^2 + \left(1 + \eta\left(\frac{5}{4}\right)^{\frac{3}{5}}\left(\frac{R}{H}\right)^2\right)^{-\frac{1}{5}} + R_e$$

where the residual can be expressed by

$$R_e = \sum_{n=1}^{\infty} a_n \frac{\left(\frac{(q+1)^{-\frac{1}{5}}-1}{q+1}\right)^n}{(q+1)^{0.2}}$$

Then, as $q \geq 0$,

$$|R_e| \leq \sum_{n=1}^{\infty} \frac{\left(\frac{1-(q+1)^{-\frac{1}{5}}}{q+1}\right)^n}{(q+1)^{0.2}} = \frac{1-(q+1)^{-0.2}}{1+q(q+1)^{0.2}} \leq 0.061 \tag{13}$$

We find that right term of Eq. (13) peaks at $q \approx 1.179$, and $|R| \to 0$ as $q \to 0$ or $q \to \infty$. Thus, V_Y/V_{Y0} can be approximated by:

$$\frac{V_Y}{V_{Y0}} = \eta\left(\frac{5}{4}\right)^{\frac{3}{5}}\left(\frac{R}{H}\right)^2 + \left(1 + \eta\left(\frac{5}{4}\right)^{\frac{3}{5}}\left(\frac{R}{H}\right)^2\right)^{-\frac{1}{5}} \tag{14}$$

In sum, we propose an estimation of V_Y/V_{Y0} as follows, with absolute error strictly not larger than 0.061. Since $V_Y/V_{Y0} \geq 1$, we could also say that Eq. (14) estimates V_Y with relative error less than 6.1%.

3.3. Modified Zener's model

To solve the nonlinear equation Eq. (1), we converted Eq. (1) into a dynamical system by letting $x_1 = \delta$ and $x_2 = \dot{\delta}$. Unlike the Hertzian model where $F(\delta)$ is bijective, a plastic model commonly has distinct loading and unloading stages. In addition, the elasto-plastic contact model includes the maximum loading displacement δ_m that determines the residual deformation δ_r. Introducing a new state variable $x_3 = \delta_m$, we can formulate a first-order dynamical system according to Eq. (1):

$$\begin{bmatrix} \dot{x_1} \\ \dot{x_2} \\ \dot{x_3} \end{bmatrix} = \begin{bmatrix} x_2 \\ -\frac{F(x_1;x_2,x_3)}{m^*} - \alpha F'(x_1;x_2,x_3)x_2 \\ \dot{x_1}\mathrm{H}(x_2) \end{bmatrix} \tag{15}$$

where $\mathrm{H}(x)$ is the Heaviside function,

$$H(x) = \begin{cases} 1 & \text{for } x \geq 0 \\ 0 & \text{for } x < 0 \end{cases}$$

and $F(x_1;x_2,x_3)$ is an equivalent piecewise function according to the NFD relationship $F(\delta)$; the domain of $F(x_1;x_2,x_3)$ can be divided into elastic loading, plastic loading, and elastic unloading stages for the MYC model (Majeed et al., 2012; Wang et al., 2017b). The NFD relationship $F(\delta)$ can be expressed as follows.

$$F(\delta) = \begin{cases} \frac{4}{3}E^* R^{*0.5}\delta^{1.5} & \text{Loading phase 1 : } \delta < \delta_P \text{ and } \dot{\delta} \geq 0 \\ \frac{4}{3}E^* R^{*0.5}\delta_p^{1.5} + 2E^* R^{*0.5}\delta_p^{0.5}(\delta - \delta_P) & \text{Loading phase 2 : } \delta \geq x_P \text{ and } \dot{\delta} \geq 0 \\ \frac{4}{3}E^* R^{*0.5}\delta^{1.5} & \text{Unloading phase 1 : } \dot{\delta} < 0 \text{ and } \delta_m < \delta_Y \\ F_m\left(\frac{\delta-\delta_r}{\delta_m-\delta_r}\right)^{1.5} & \text{Unloading phase 2 : } \dot{\delta} < 0 \text{ and } \delta_m \geq \delta_Y \end{cases} \tag{16}$$

where F_m is the maximum force during loading stage and the residual deformation δ_r is determined by

$$\delta_r = \delta_m - \delta_Y\left(2\frac{\delta_m}{\delta_Y} - 1\right)^{0.5} \tag{17}$$

In Eq. (16), the phase-dividing parameters, δ_Y and δ_P can be calculated using

$$\begin{cases} \delta_Y = \frac{0.68\pi^2\sigma_Y^2 R^*}{E^{*2}} \\ \delta_P = \frac{2.14\pi^2\sigma_Y^2 R^*}{E^{*2}} \end{cases} \tag{18}$$

Using variable x_1, x_2, and x_3, the MYC model for the dynamical system Eq. (15) can be rewritten as

$$F(x_1;x_2,x_3) = \begin{cases} \frac{4}{3}E^*R^{*0.5}x_1^{1.5} & x_1 < \delta_P \text{ and } x_2 \geq 0 \\ \frac{4}{3}E^*R^{*0.5}\delta_p^{1.5} + 2E^*R^{*0.5}\delta_p^{0.5}(x_1-\delta_p) & x_1 \geq \delta_P \text{ and } x_2 \geq 0 \\ \frac{4}{3}E^*R^{*0.5}x_1^{1.5} & x_2 < 0 \text{ and } x_3 < \delta_Y \\ F_m\left(\frac{x_1-\delta_r}{x_3-\delta_r}\right)^{1.5} & x_2 < 0 \text{ and } x_3 \geq \delta_Y \end{cases} \tag{19}$$

and the derivative of $F(x)$ as

$$F'(x_1;x_2,x_3) = \begin{cases} 2E^*R^{*0.5}x_1^{0.5} & x_1 < \delta_P \text{ and } x_2 \geq 0 \\ 2E^*R^{*0.5}\delta_p^{0.5} & x_1 \geq \delta_P \text{ and } x_2 \geq 0 \\ 2E^*R^{*0.5}x_1^{0.5} & x_2 < 0 \text{ and } x_3 < \delta_Y \\ \frac{3}{2}\frac{F_m}{x_3-x_1}\left(\frac{x_1-\delta_r}{x_3-\delta_r}\right)^{0.5} & x_2 < 0 \text{ and } x_3 \geq \delta_Y \end{cases} \tag{20}$$

With Eqs. (15) and (17)-(20), the dynamical system can be solved with Runge-Kutta method (Dormand and Prince, 1980; Shampine, 1986).

3.4. Semi-analytical solution for COR

Taking the elastoplastic γAl_2O_3 sphere impacting elastic glass plate as an example, with present modified Zener's model, we investigated the effects of impact velocity and plate thickness on the COR. Solving Eq. (15), we obtained the COR as a function of the dimensionless plate thickness (R/H) and the dimensionless impact velocity (V_0/V_{Y0}), as a shown in Fig. 5A. The surface in Fig. 5A clearly shows that the COR decreases as the impact velocity increases, or as the plate becomes thinner. Fig. 5B shows a detailed comparison of predicted COR between Muller's model (Mueller et al., 2015) (a linearization to Zener's model) and present model. We find that Mueller's model significantly overestimates the COR for $V_0 > V_Y$. If the impact velocity V_0 exceeds the yielding velocity V_Y, besides the flexural wave, the plastic dissipation also accounts for the kinetic energy loss of the sphere. In Mueller's model, since only elastic contact was considered, a distinguishable overestimation can thus be found.

Practically, an explicit expression for the COR, rather than an implicit dynamical system, can bring much more convenience. To obtain an explicit expression, we employed the following semi-analytical approach.

First of all, we check the thickness-dependent yielding velocity in Eq. (14) with the results integrated with present model, shown in Fig. 6. The error is less than 1.2%, which agrees with the estimation of residual $|R_e| \leq 0.061$.

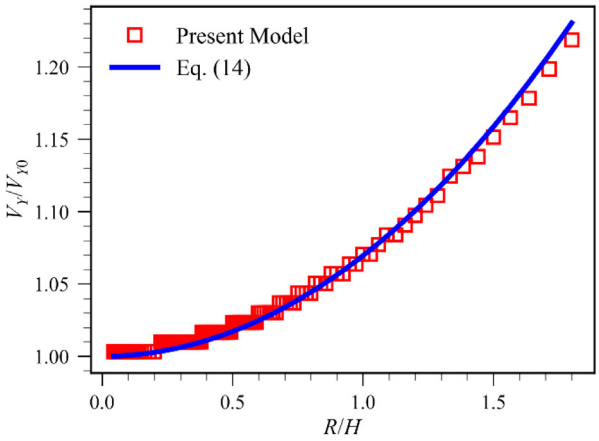

Fig. 6. Dimensionless yielding impact velocity as function of dimensionless plate thickness.

Next, for the COR that depends on R/H and V_0/V_Y, the COR must degenerate to its trivial form (bulk case) as $H \to \infty$. The trivial form can be obtained by direct integrating the loading curve and the unloading curve in the MYC model.

$$\lim_{\frac{R}{H}\to 0} e = \left(1-\left(1-\left(\frac{V_0}{V_{Y0}}\right)^{-\frac{4}{5}}\right)^2\right)^{\frac{1}{4}} \tag{21}$$

To account for the effect of thickness, we mutate the power index with a polynomial function of R/H. Optimization according to the surface of Fig. 5 with least square method, we can obtain the explicit form for the COR:

$$e = \begin{cases} \exp\left(-\pi\frac{\lambda}{\sqrt{4-\lambda^2}}\right) & \text{elastic : if } \frac{V_0}{V_{Y0}} \leq g \\ \left(1-\left(1-\left(\frac{1}{g}\frac{V_0}{V_{Y0}}\right)^{-\frac{4}{5}}\right)^2\right)^{\frac{1}{4}+c\left(\frac{R}{H}\right)^2} & \text{plastic : if } \frac{V_0}{V_{Y0}} > g \end{cases} \tag{22}$$

where

$$g = \eta\left(\frac{5}{4}\right)^{\frac{3}{5}}\left(\frac{R}{H}\right)^2 + \left(1+\eta\left(\frac{5}{4}\right)^{\frac{3}{5}}\left(\frac{R}{H}\right)^2\right)^{-\frac{1}{5}}$$

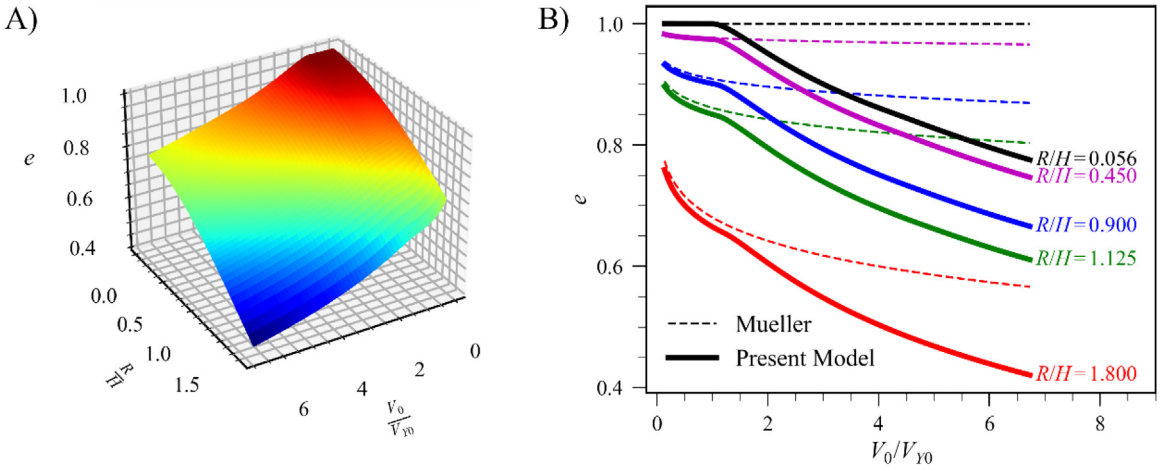

Fig. 5. A) Coefficient of restitution as function of dimensionless impact velocity and dimensionless plate thickness. B) Comparison of present model to Mueller's model under different plate thickness.

and

$c = 0.0935$

4. Result and discussion

4.1. Verification of the semi-analytical solution for COR

We conducted a FEM simulation to verify the semi-analytical solution Eq. (22). Without loss of generality, we took an elastoplastic sphere (γAl_2O_3) impacting a sufficiently large elastic plate (glass) as an example. A FEM model with explicit dynamic solver was adopted for the simulation, in which the initial velocity V_0 and the plate thickness H were varying parameters. Details can be found in Appendix.

First, we show that traditional models, such as Raman's model (Raman, 1920), Zener's model (Zener, 1941), and Mueller's model (Mueller et al., 2015), will fail when plastic deformation occurs. Fig. 7 compared these models with the FEM results, showing that: although Raman's and Zener's models can predict the COR in the purely elastic regime, they overestimate the COR when the plastic deformation occurs. For a small value of λ, a relative error of such overestimation is above 20%, shown in the inset of Fig. 7.

Next, we compared our semi-analytical solution Eq. (22) with the FEM results, shown in Fig. 8. The overall trend by Eq. (22) is in good agreement with that by the FEM results. The margin of error becomes relatively larger (up to 14%) for thin plate, e.g., $H = 0.556R$. The reason maybe that the geometry nonlinearity must be considered for thin plates to formulate the flexural wave. In conclusion, present semi-analytical solution can be used to predict the coefficient of restitution for a range of thickness ($H \geq 0.556R$) under an impact velocity lower than $7V_{Y0}$ within a maximum error less than 14%.

4.2. Energy dissipation by plasticity

With the present modified Zener's model, we can quantitatively study how contact plasticity affects the fractions of the kinetic energy loss of the sphere. The loss of kinetic energy, ΔE, composes of two parts: the flexural energy transferred from the sphere to the plate and the energy dissipated by plasticity E_p. By solving the present modified Zener's model, we can obtain the history of the compressive relative displacement. Using the force-compressive relative displacement relationship of the MYC model, we can calculate the plastic dissipation by integration. Then, the energy loss due to flexural wave can be obtained by subtracting the dissipation by plasticity from the kinetic energy loss of the sphere. The phase diagram in Fig. 9A shows the contour of COR as a function of dimensionless thickness R/H and dimensionless impact velocity V_0/V_{Y0}. The isolines labelled with $E_p/\Delta E = 0$ and $E_p/\Delta E = 0.5$ divides the whole domain into three distinct regions, labelled with I, II, and III, respectively. Region I is the elastic region, in which the kinetic energy loss of the sphere is solely due to the flexural wave. The traditional models, such as Raman's model, Zener's model, and Mueller's model, are only valid in region I. In region II and III, the energy loss is composed of flexural wave and plastic dissipation: region II is dominant by flexural wave, while region III is dominant by plastic dissipation. Numerical fitting shows that the borderline between region II and III can be expressed by

$$\left(\frac{V_0}{V_{Y0}}\right)^{\frac{2}{5}} = 1 + 1.001\left(\frac{R}{H}\right)^2 \tag{23}$$

With such phase diagram (Fig. 9A), we are able to visualize the state of the impact condition to determine whether plasticity should be considered, or whether plastic dissipation will be the dominant one against flexural wave. For instance, we plotted in Fig. 9A the states of the experiments carried out by Mueller et al. (Mueller et al., 2015), Patil and Higgs (Patil and Higgs, 2017), and Kharaz and Gorham (Kharaz and Gorham, 2000). Muller et al. experimented on elastic impact of γAl_2O_3 bead on glass plate, so the states locate in region I; Kharaz and Gorham experimented on the plastic dissipation of aluminum oxide sphere impacting steel plate, so the states locate in region II; Patil and Higgs experimented on the elastoplastic impact of tungsten sphere on aluminum plate, so the states span over region II and region III.

As an example, we check the thickness effect on the energy partitions. Fig. 9B, a stacking plot, shows the energy partition as a function of impact velocity for $R/H = 0.2$, 0.5 and 1.2. For a thin plate ($R/H = 1.2$), in current range of impact velocity, plastic dissipation will never dominant the energy loss of the sphere. For a plate with $R/H = 0.5$, as the impact velocity increases, the main role controlling the kinetic energy loss shifts from flexural wave to plastic dissipation. For a thick plate ($R/H = 0.2$), the contact force is not likely to produce significant deformation to the plate.

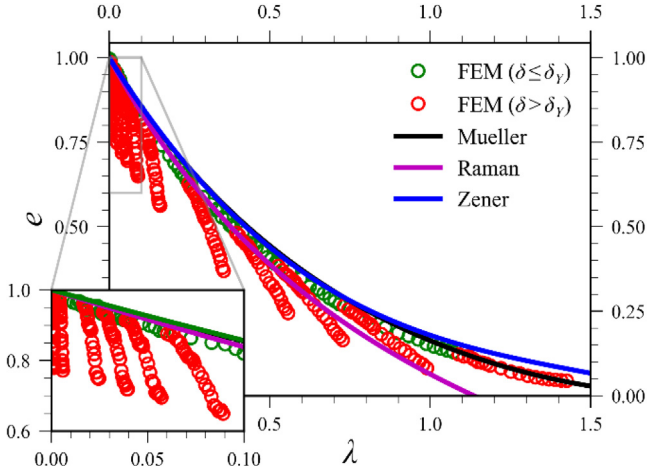

Fig. 7. Coefficient of restitution as a function of λ. Results from FEM simulation is plotted as circles. Green ones represent cases where deformation is purely elastic and red ones represent cases where plastic deformation occurs. (For interpretation of the references to colour in this figure legend, the reader is referred to the web version of this article.)

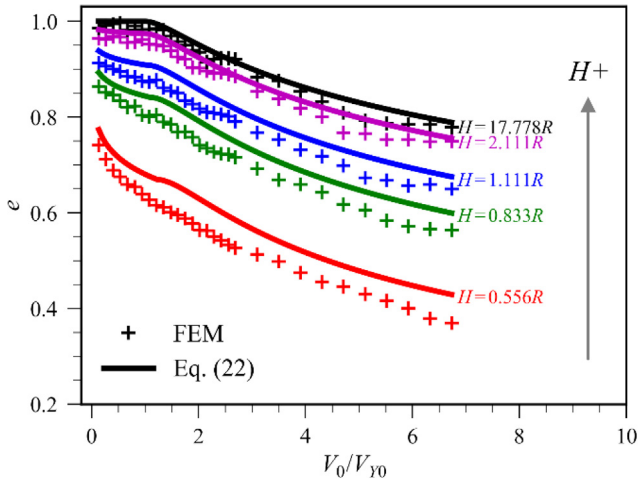

Fig. 8. Validation of the semi-analytical solution for COR with the results by FEM simulations.

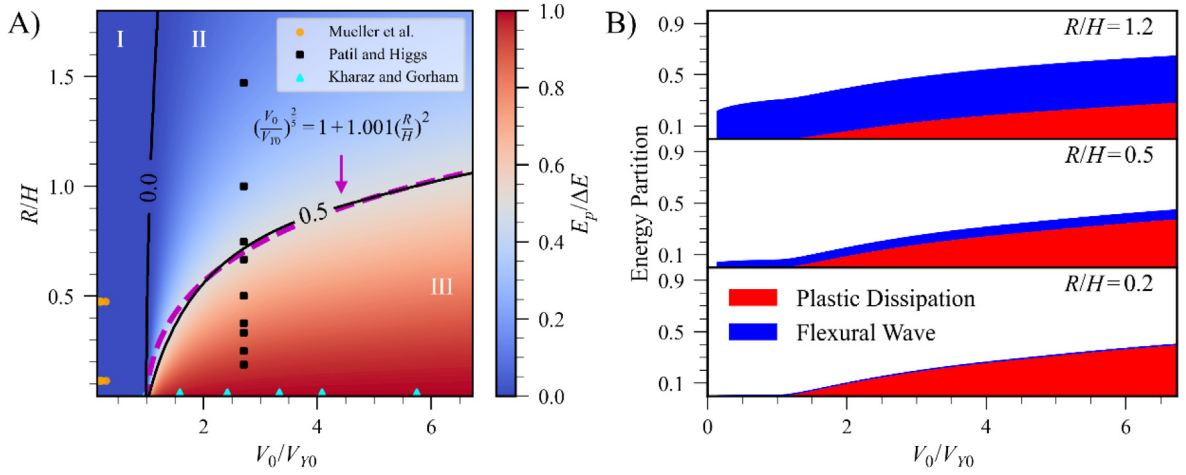

Fig. 9. A) Contour of ratio of plastic dissipation to kinetic energy loss as function of dimensionless impact velocity and dimensionless thickness. B) Stack plot for energy partition (ratios of plastic dissipation and flexural wave to total kinetic energy) as function of dimensionless velocity.

Consequently, as the impact velocity exceeds the critical velocity V_Y, the plastic dissipation becomes the only cause to the kinetic energy loss if we ignore the insignificant flexural wave.

4.3. Effects of plate thickness on contact duration

Contact duration is also important during the dynamic contact for applications such as electrical switch or trigger. Is the duration the same for the case of bulk and plate? In addition, does the plasticity also affect the contact duration? Fig. 10 plots the contact duration for various impact velocities and plate thicknesses. First, given an impact velocity, thinner plate means greater compliance of the plate to the motion of the sphere, which, in turn, elongates the contact duration. Second, given a plate thickness, the larger the impact velocity is, the shorter the contact duration is. This result agrees with the fact that for a Hertzian contact, the contact duration $t_d \propto \left(m^*/V_0^{0.5}\right)^{0.4}$ (Love, 1944; Zener, 1941). Third, comparison between current models and the FEM simulations shows that the present model is capable of predicting the contact duration, whilst Zener's model may slightly overestimate the contact duration if plastic deformation takes place. Last, the trends shown in Fig. 10 indicates that plasticity affects contact duration to only a small extent compared with Zener's model.

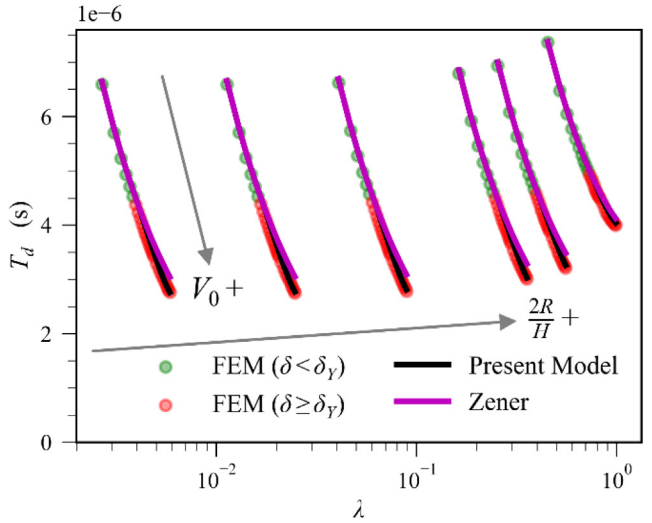

Fig. 10. Contact time T_d as function of λ.

4.4. Limitations of present model

The limitations of the present model are as follows. One aspect is of strain-rate effect. Previous studies have shown that for some materials, strain-rate plays a significant role in contact process, such as a steel sphere impacting on a steel plate (Jin et al., 2020) and shot-peening impacts (Alfredsson and Nordin, 2013). In such cases, a new model is required to model the dynamic contact of materials with strain-rate dependence. However, at present there is no universal contact law considering rate effect. Another aspect of the limitation is of contact viscosity. For some high-speed impact cases, contact viscosity may accounts for a large fraction of energy loss. Many models use a velocity-dependent hysteresis damping factor to model the contact viscosity, such as the L-N model (Lankarani and Nikravesh, 1990) and the Flores model (Flores et al., 2011). Flores and Lankarani summarized over 15 different types of dissipative contact force models (Flores and Lankarani, 2016); there is also no universal dissipative contact force model. As a result, in the present study, as long as the MYC model fits the contact behavior of the contact pairs, the present model will be acceptable.

In addition, Russell experimentally studied the effect of a deformable coating layer on the sphere and its thickness on elasto-

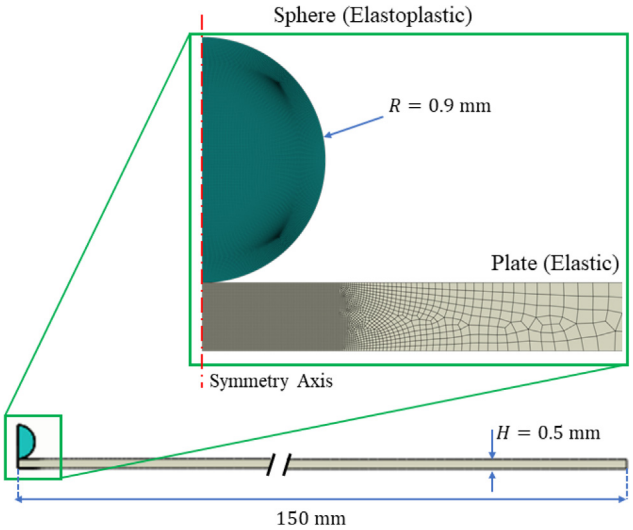

Fig. 11. FEM model for an elastoplastic sphere impacting an elastic plate.

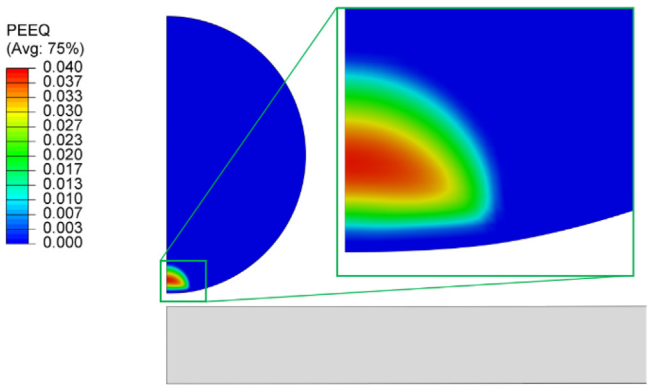

Fig. 12. Distribution of plastic strain after sphere is detached from plate.

plastic COR (Russell, 2020). Due to the existence of the coating on the sphere, the contact law may differ. In that situation, Zener's equation must be modified with a suitable contact law instead of the MYC contact law. Further, when the plate is too thin, the geometry nonlinearity must be considered, but Zener's equation cannot consider this. Thus, we believe in this case a more accurate model is required, and this question remains open.

5. Conclusion

Considering contact plasticity, we proposed a modified Zener's model to study an elastoplastic sphere impacting an elastic plate. The conclusions are as follows:

1. We obtained an explicit expression of the yielding velocity for a plastic sphere impacting on an elastic plate, the yielding velocity by Eq. (14) shows nonlinear dependency on the thickness of plate, with error less than 6%.
2. Employing MYC plastic model into the control equation, we developed a modified Zener's model to study the elastoplastic impact on a plate. With the developed model, we presented a semi-analytical solution Eq. (22) for the prediction of COR,

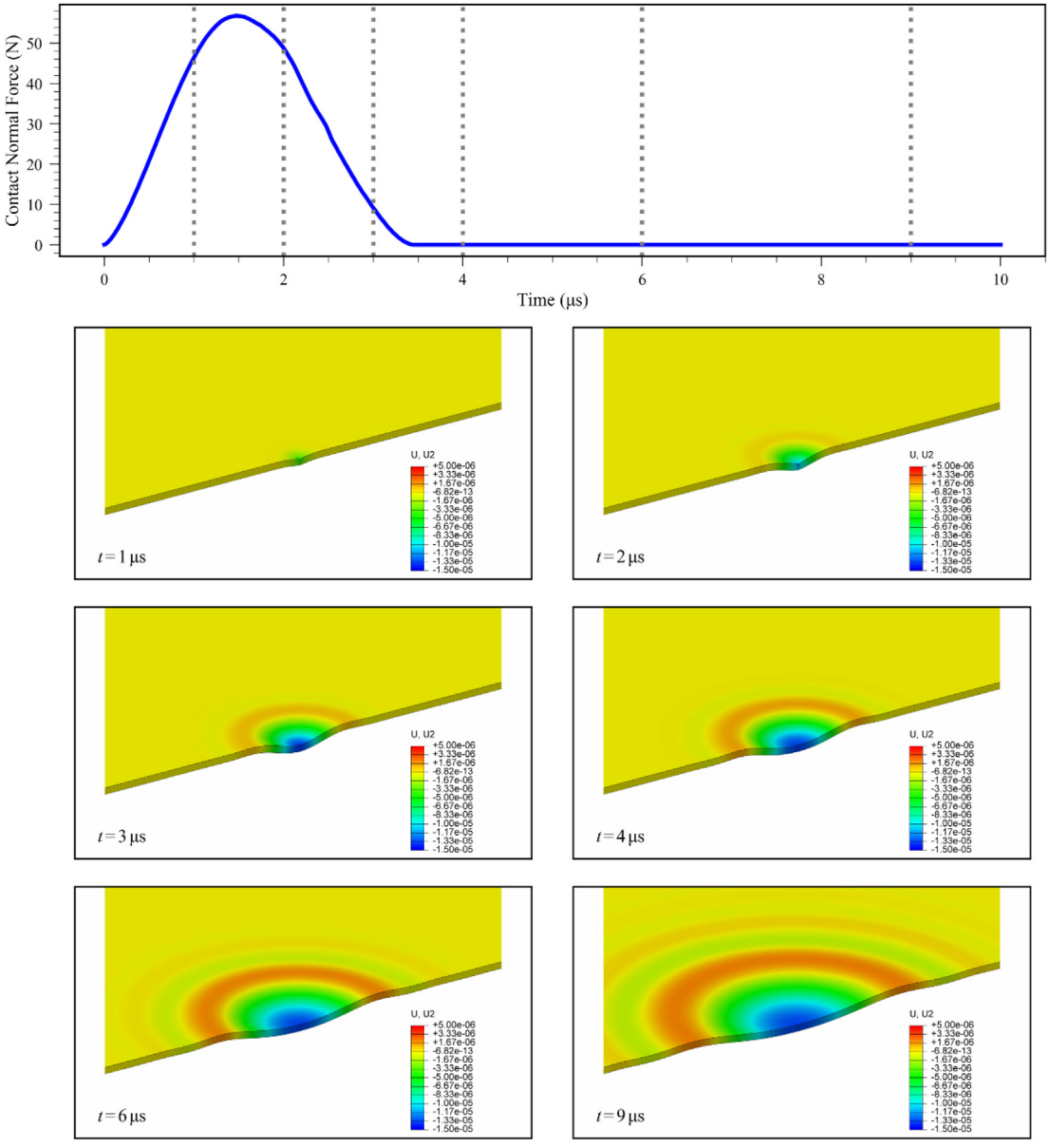

Fig. 13. Deformation of the plate at typical times.

which can well predict the transition from elastic to elastoplastic impact on a plate. This solution can be used for the thin plate whose thickness ratio H/R is larger than 0.556.

3. Results show that energy loss during the sphere-plate impact can be divided into three zones in the phase diagram with respect to velocity and thickness: zones dominated by elastic deformation, by flexural wave, and by plastic dissipation. The borderline of the latter two zones is presented as Eq. (23) and shown in Fig. 9. In addition, we found that the effect of contact plasticity on contact duration can be ignored.

Declaration of Competing Interest

The authors declare that they have no known competing financial interests or personal relationships that could have appeared to influence the work reported in this paper.

Acknowledgement

This work was supported by the National Natural Science Foundation of China (No. 12022210, 12032001, 11772334, 11890681), by the Youth Innovation Promotion Association CAS (2018022), by the Strategic Priority Research Program of the Chinese Academy of Sciences (No. XDB22040501).

Appendix:. FEM simulation

FEM simulations were conducted using ABAQUS commercial software (Dassualt Systèmes, Vélizy-Villacoublay, France) with a dynamic solver (ABAQUS/Explicit). Due to the symmetry, only an axisymmetric model was necessary, shown in Fig. 11. The radius of the sphere R was set to 0.9 mm. The radius of the plate was set to 150 mm, sufficiently large to eliminate boundary effects (possible wave reflection). A contact pair was established between the sphere and the plate: the penalty method of constraint enforcement was applied on the normal direction for the pressure-overclosure relationship ('Hard' contact in ABAQUS), and the friction coefficient was set to 0.1. The materials for the elastic-perfect plastic sphere and the elastic plate are γAl_2O_3 and glass, respectively. Detailed material parameters are listed in Table 1. The element (CAX4R) count in this model was about 23000, with the finest element size at the contact region being $1\%R$. To investigate energy partitions, kinetic energy, elastic strain energy, and plastic dissipation of the sphere were request for result output, as well as the elastic strain energy and kinetic energy of the plate. We parametrically studied the cases with various impacting velocity and plate thicknesses. Fig. 11 shows the model with plate thickness $H = 0.5$mm and impact velocity $V_0 = 26$m/s as an example.

Fig. 12 shows the distribution of equivalent plastic strain after the sphere is detached from the plate. The highest plastic strain is about 0.039. It is evident that a fraction of the kinetic energy is dissipated by plastic deformation.

To see how the plate deforms, we scaled the deformation scale factor to 50 since the deformation was actually too small to be visualized. Fig. 13 shows the history of the contact force, which can be treated as an indicator for the status of sphere/plate contact: at time $t = 1, 2, 3\mu$s, the sphere is in touch with the plate. The contours in Fig. 13 visualize the vertical displacement of the plate at various times. It can be seen that the flexural wave travels away from the impact center like a ripple, and no reflective wave can be observed during the whole impact process.

References

ABAQUS, 2016. ABAQUS Documentation, Version 2016. Dassault Systèmes.
Alfredsson, B., Nordin, E., 2013. An elastic-plastic model for single shot-peening impacts. Tribol. Lett. 52 (2), 231–251.
Boettcher, R., Russell, A., Mueller, P., 2017. Energy dissipation during impacts of spheres on plates: Investigation of developing elastic flexural waves. Int. J. Solids Struct. 106-107, 229–239.
Brake, M.R., 2012. An analytical elastic-perfectly plastic contact model. Int. J. Solids Struct. 49 (22), 3129–3141.
Brake, M.R.W., 2015. An analytical elastic plastic contact model with strain hardening and frictional effects for normal and oblique impacts. Int. J. Solids Struct. 62, 104–123.
Davies, R.M., 1949. The determination of static and dynamic yield stresses using a steel ball. Proc. R. Soc. Lond. Ser. A Math. Phys. Sci. 197, 416–432.
Dong, X., Yin, X., Deng, Q., Yu, B.o., Wang, H., Weng, P., Chen, C., Yuan, H., 2018. Local contact behavior between elastic and elastic-plastic bodies. Int. J. Solids Struct. 150, 22–39.
Dormand, J.R., Prince, P.J., 1980. A family of embedded Runge-Kutta formulae. J. Comput. Appl. Math. 6 (1), 19–26.
Flores, P., Lankarani, H.M., 2016. Contact Force Models for Multibody Dynamics, Solid Mechanics and Its Applications. Springer International Publishing, Cham.
Flores, P., Machado, M., Silva, M.T., Martins, J.M., 2011. On the continuous contact force models for soft materials in multibody dynamics. Multibody Sys. Dyn. 25 (3), 357–375.
Ghaednia, H., Marghitu, D.B., Jackson, R.L., 2015. Predicting the permanent deformation after the impact of a rod with a flat surface. J. Tribol. Trans. ASME 137, 8.
Hunter, S.C., 1957. Energy absorbed by elastic waves during impact. J. Mech. Phys. Solids 5 (3), 162–171.
Hutchings, I.M., 1979. Energy absorbed by elastic-waves during plastic impact. J. Phys. D Appl. Phys. 12 (11), 1819–1824.
Jackson, R.L., Green, I., 2005. A finite element study of elasto-plastic hemispherical contact against a rigid flat. J. Tribol. Trans. ASME 127, 343–354.
Jin, T., Yin, X., Zhang, L., Wang, H., Yu, B.o., Hao, Q., 2020. Strain-rate-dependent model for the elastoplastic dynamic contact of sphere and plate. Mater. Res. Express 7 (6), 066523. https://doi.org/10.1088/2053-1591/ab9ae5.
Johnson, K.L., 1985. Contact Mechanics. Cambridge University Press, Cambridge Cambridgeshire New York.
Kharaz, A.H., Gorham, D.A., 2000. A study of the restitution coefficient in elastic-plastic impact. Philos. Mag. Lett. 80 (8), 549–559.
Kogut, L., Etsion, I., 2002. Elastic-plastic contact analysis of a sphere and a rigid flat. J. Appl. Mech. Trans. ASME 69, 657–662.
Kogut, L., Komvopoulos, K., 2004. Analysis of the spherical indentation cycle for elastic-perfectly plastic solids. J. Mater. Res. 19 (12), 3641–3653.
Koller, M.G., Kolsky, H., 1987. Waves produced by the elastic impact of spheres on thick plates. Int. J. Solids Struct. 23 (10), 1387–1400.
Landau, L.D., Lifshi͡ts, E.M., Kosevich, A.M., Pitaevskiĭ, L.P.,, 1986. Theory of Elasticity. Pergamon Press, Oxford Oxfordshire, New York.
Lankarani, H.M., Nikravesh, P.E., 1990. A contact force model with hysteresis damping for impact analysis of multibody systems. J. Mech. Des. 112, 369–376.
Love, A.E.H., 1944. A Treatise on the Mathematical Theory of Elasticity. Dover Publications, New York.
Majeed, M.A., Yigit, A.S., Christoforou, A.P., 2012. Elastoplastic contact/impact of rigidly supported composites. Compos. Part B Eng. 43 (3), 1244–1251.
Majumdar, A., Bhushan, B., 1991. Fractal model of elastic-plastic contact between rough surfaces. J. Tribol. Trans. ASME 113, 1–11.
Mittal, R.K., 1987. A simplified analysis of the effect of transverse-shear on the response of elastic plates to impact loading. Int. J. Solids Struct. 23 (8), 1191–1203.
Mueller, P., Boettcher, R., Russell, A., Truee, M., Tomas, J., 2015. A novel approach to evaluate the elastic impact of spheres on thin plates. Chem. Eng. Sci. 138, 689–697.
Müller, P., Böttcher, R., Russell, A., Trüe, M., Aman, S., Tomas, Jürgen, 2016. Contact time at impact of spheres on large thin plates. Adv. Powder Technol. 27 (4), 1233–1243.
Patil, D., Higgs, C.F., 2017. A coefficient of restitution model for sphere-plate elastoplastic impact with flexural vibrations. Nonlinear Dyn. 88 (3), 1817–1832.
Peng, Q., Ye, X., Wu, H., Liu, X., Wei, Y.G., 2020. Effect of plasticity on dynamic impact in a journal-bearing system: A planar case. Mech. Mach. Theory 154, 104034. https://doi.org/10.1016/j.mechmachtheory.2020.104034.
Raman., C.V., 1920. On some applications of Hertz's theory of impact. Phys. Rev. 15 (4), 277–284.
Reed, J., 1985. Energy-losses due to elastic wave-propagation during an elastic impact. J. Phys. D-Appl. Phys. 18 (12), 2329–2337.
Russell, A., 2020. On the Mechanical Behavior of Coarse particulate Products. University of Magdeburg.
Shampine, L.F. 1986. Some practical Runge-Kutta formulas. Math. Comput. 46, 135–150.
Sherif, H.A., Almufadi, F.A., 2018. Analysis of elastic and plastic impact models. Wear 412-413, 127–135.

Stronge, W.J., 2000. Contact problems for elasto-plastic impact in multi-body systems. Impacts Mech. Syst. Anal. Modell. 551, 189–234.
Stronge, W.J., 2019. Impact Mechanics. University of Cambridge, Cambridge, United Kingdom; New York, NY, USA.
Thornton, C., 1997. Coefficient of restitution for collinear collisions of elastic perfectly plastic spheres. J. Appl. Mech. Trans. ASME 64, 383–386.
Wang, H., Yin, X., Deng, Q., Yu, B., Hao, Q., Dong, X., 2017a. Experimental and theoretical analyses of elastic-plastic repeated impacts by considering wave effects. Eur. J. Mech. A Solids 65, 212–222.
Wang, H., Yin, X., Qi, X., Deng, Q., Yu, B., Hao, Q., 2017b. Experimental and theoretical analysis of the elastic-plastic normal repeated impacts of a sphere on a beam. Int. J. Solids Struct. 109, 131–142.
Wu, C.-Y., Li, L.-T., Thornton, C., 2003. Rebound behaviour of spheres for plastic impacts. Int. J. Impact Eng. 28 (9), 929–946.
Wu, C.-Y., Li, L.-Y., Thornton, C., 2005. Energy dissipation during normal impact of elastic and elastic-plastic spheres. Int. J. Impact Eng. 32 (1-4), 593–604.
Ye, N., Komvopoulos, K., 2003. Indentation analysis of elastic-plastic homogeneous and layered media: Criteria for determining the real material hardness. J. Tribol. Trans. ASME 125, 685–691.
Ye, X., Hu, J., Song, J., Liu, X., Wei, Y., 2020. Semi-analytical model of the vertical impact of a 316 stainless steel rod. Int. J. Impact Eng. 146, 103694. https://doi.org/10.1016/j.ijimpeng.2020.103694.
Zener, C., 1941. The intrinsic inelasticity of large plates. Phys. Rev. 59 (8), 669–673.